AIAS 2018 International Conference on Stress Analysis

# A possible use of SMArt thermography for the control of GFRP composite laminate

De Giorgi M.[a], Nobile R.[a]*

[a]*Department of Engineering for Innovation, University of Salento, Via Arnesano, 73100 Lecce, Italy*

**Abstract**

The development of techniques able to check the structural health of a wind blade is very important. An innovative and promising technique applicable at this aim is the SMArt thermography. It exploits the electro-thermal properties of SMArt composites, in order to detect the structural flaws using an embedded source. Such a system enables a built-in, fast, cost-effective and in-depth assessment of the structural damage as it overcomes the limitations of standard thermography.

With the aim for developing a reliable diagnostic method based on SMArt thermography, a preliminary numerical model was implemented in order to simulate the heating and the subsequent cooling of a GFRP composite laminate with embedded SMA wires. The heat source was represented by the Joule effect originated in the SMA wires and supplied as power density. The analysis of the resulting thermal maps at different values of power density provided the optimal levels of current amplitude and period to be applied in the subsequent experimental applications.

## 1. Introduction

The reduction of the cost of energy produced by large dimension wind blades can be achieved improving their lifetime and enabling them to optimize power production without suffering mechanical failure.

---

* Corresponding author. Tel.: +39-832-297772; fax: +39-832-297768.
E-mail address: riccardo.nobile@unisalento.it

The structural health of a wind blade, therefore its operating life, is conditioned during its whole life by initial defects, and defects arising after installation under environmental loading condition. Any difference of the real operating conditions with respect to those statistically estimated and used for design is a potential source of damage, possibly leading to a fault or a lifetime reduction. Therefore, the development of techniques able to check the structural health of a wind blade is very important. An innovative and promising technique applicable at this aim is the SMArt thermography. It exploits the electro-thermal properties of multifunctional smart structures, realised embedding Shape Memory Alloy (SMA) wires in traditional carbon or glass fiber reinforced composite laminates known as SMArt composites, in order to detect the structural flaws using an embedded source. Such a system enables a built-in, fast, cost-effective and in-depth assessment of the structural damage as it overcomes the limitations of standard thermography.

**Nomenclature**

| | |
|---|---|
| k | thermal conductivity |
| C | volumetric thermal capacity |
| h | natural convection coefficient |
| $\Delta T$ | temperature difference between surface and air |
| L | characteristic dimension of the exchanging surface |
| $\rho$ | linear resistance of the wire |
| d | wire diameter |
| I | electrical current |
| S | power density |

The insertion of SMA wires in a composite structure could lead to several advantages: first of all, enhanced mechanical properties can be reached. A comprehensive review about this scope is reported in Angioni et al. (2011). On the contrary, the use of SMA to obtain additional non-structural functions is reported only in few works. For example, SMA have been used as strain sensing integrated in the composite to evaluate the amount of damage in a GFRP panel by measuring the variation of electrical resistance of embedded NiTi wires (Nagai and Oishi (2006)). In order to use SMA as a strain sensor Cui et al. (2010) showed that the material must be in its martensitic form in order to obtain a linear relation between electrical resistance and strain and independent from temperature. Finally, the acoustic emission signals generated from the austenite/martensite phase change has been used to localize the extent of damaged areas and the level of strain field that originated the damage, as reported by Oishi and Nagai (2005).

In the present work, the idea is to verify the possibility to use SMA wires embedded in a composite panel to improve the damage detection capabilities of Active Infrared Thermography, which represents a widely used non-destructive technique able to detect subsurface defects for a wide variety of structural homogeneous and composite materials (Pickering and Almond (2008)). A critical point of the Active Thermography is represented by the need of an external thermal stimulation, which will provide a uniform heating of the component under investigation followed by a natural cooling. Observing the spatial temperature gradient using an infrared camera is then possible to detect thermal irregularities that could be associated to initial defect, damage induced by stress state or impact, etc. and providing in general useful information about the structural integrity of the component. Thermal irregularities are, in fact, originated by differences existing in heat exchange conditions between damaged and undamaged zones (Carslaw and Jaeger (1959), Maldague (2002)). As a consequence, the thermal contrast can be used to locate invisible defects embedded within the material and to measure their extent. Thermography can detect cracks in Glass Fibre Reinforced Plastics (GFRP) composites and it has been also proved to give good results in detecting voids, inclusions, and impact damage in Carbon Fibre Reinforced Plastics (CFRP) laminates (McLaughlin et al. (1980)).

The external stimulation of Active Thermography could be potentially obtained using a wide variety of techniques. However, the most simple and used is constituted by halogen lamps, but the heating could be not uniform, especially if a large component is considered. For this reason, the definition of the optimal set-up measurement can be high-time consuming and in several cases not completely adequate. Starting from these

consideration, it is evident the advantages that an internal and diffused thermal source embedded in a complex component could constitute. A schematic set-up of this novel technique is represented in Fig. 1, compared with the traditional thermography.
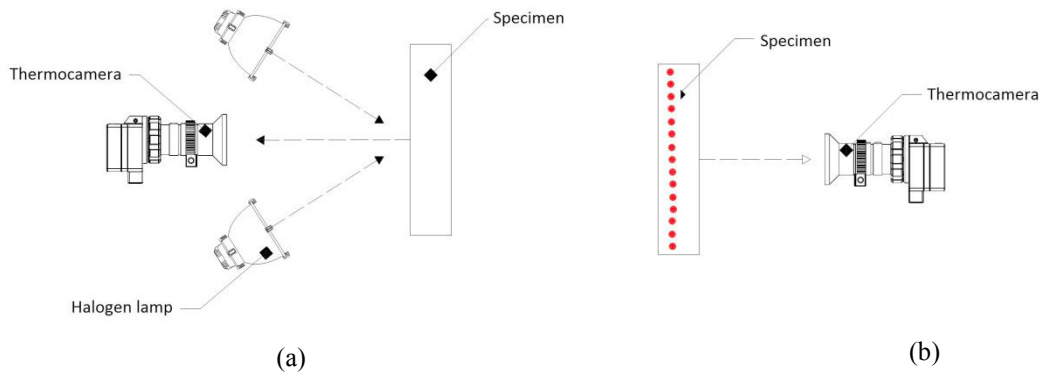


Fig. 1. Schematics of traditional active thermography (a) and material enabled thermography (b).

The results of a recent application of this techniques to panels in CFRP is reported in Pinto et al. (2014), Angioni et al. (2016), which experimentally studied the influence of several factors on the sensitivity and resolution of the technique. In particular, authors observed that internal delaminations can be spotted easily by analyzing the thermograms acquired from an IR-Camera, giving good results in terms of position and spatial extent. Increasing the intensity of the current flowing through each embedded wire it is possible to increase the resolution of the system. The sensitivity can be further tuned scanning selected portion of the structure by changing the number of wires used for the inspection and exploiting the insulating properties of the resin, thus lowering the total power requirements. Moreover, because the superficial thermal contrast is strongly affected by the time required for the propagation of the heat wave through the defect, the relative position between different damaged areas along the thickness can be evaluated.

## 2. Materials and methods

With the aim for developing a reliable diagnostic method based on SMArt thermography to be used for the control of wind blades, a preliminary numerical model was implemented in order to simulate the heating and the subsequent cooling of a GFRP composite laminate with embedded SMA wires. The heat source was represented by the Joule effect originated in the SMA wires and supplied as power density S [W/m$^3$]. The analysis of the resulting thermal maps at different values of power density provided the optimal levels of electrical current and time to be applied in the subsequent experimental applications.

The numerical analysis was performed using the open source FEM software Code-Aster. The first step consisted in modelling a unit cell of the unidirectional 0° laminate containing two plies and an embedded SMA wire. The laminate is a unidirectional GFRP, which is commonly used for the realization of wind blades. The SMA wire is made of Flexinol ® and has a diameter of 0.25 mm. The global dimensions of the unit cell were 5x2x1mm, which was meshed using hexahedral elements HEXA8 and consisted of 2685 nodes and 2048 elements (Fig. 2).

The thermal properties to be assigned to the material for a transient linear analysis were the thermal conductivity k [W/(mK)] and the volumetric thermal capacity C [J/(m$^3$K)].

Thermal conductivity of a fiber-reinforced polymer depends on the fiber type, orientation, fiber volume fraction and lamination configuration. With the exception of carbon fibers, fiber-reinforced polymers have in general low thermal conductivity. For unidirectional 0° composites, the longitudinal thermal conductivity is controlled by the fibres, while the transverse thermal conductivity is controlled by the matrix. This is reflected in widely different values of thermal conductivity in these two directions (Mallick (2007)).
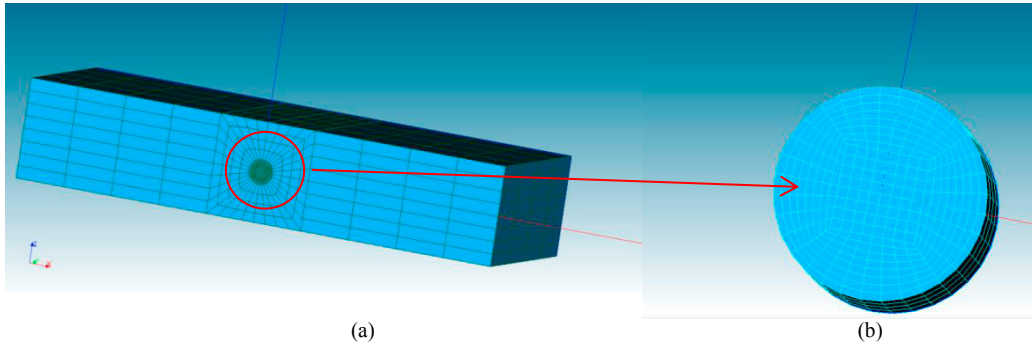
Fig. 2. FEM model of unit cell with a SMA wire (a), detail of the SMA wire (b).

The values of the thermal conductivity and volumetric thermal capacity for the different materials of the model have been assumed on the basis of literature data (Dattoma et al. (2013), Bai et al. (2008)) and technical sheet for SMA wires (Gorbet et al. (1998), Flexinol ® Technical and Design Data (2018)). The initial temperature of the entire model was imposed equal to 20°C. These values are reported in the following Table 1.

Table 1. Thermal properties of materials

|  |  | E-glass | SMA wires |
|---|---|---|---|
| $k_l$ -Thermal conductivity – longitudinal direction | [W/(mK)] | 1.3 | 18 |
| $k_t$ - Thermal conductivity – transversal direction | [W/(mK)] | 0.21 | - |
| C – volumetric thermal capacity | [J/(m³K)] | 1440000 | 53568 |

Finally, an estimation of the heat convention transfer coefficient is needed to define the thermal properties of the model. Since the panel will be subjected to natural convention in air and the superficial temperature will be close to room temperature, the heat convention transfer coefficient h can be calculated using the simplified formula reported in Krasnoshchekov and Sukomel (1978):

$$h=1.32\left(\frac{\Delta T}{L}\right)^{\frac{1}{4}}$$

(1)

where $\Delta T$ is the difference between the wall and fluid temperature that has been assumed, L is the characteristic dimension of the exchanging surface. Assuming $\Delta T$ equal to 20 K and substituting the values in (1), the heat convention transfer coefficient h is assumed equal to 10.5 W/(m²K).

The thermal load was applied as power density on the SMA wire. In order to obtain an indication of the power density needed to produce a temperature increase of about 10-20 K, a first-order heating model accounting for Joule-heating and convection (Ma et al. (2009)) was applied to approximate the expected steady-state temperature of the wire:

$$\Delta T=\frac{\rho}{h\cdot\pi\cdot d}\,I^2$$

(2)

where *I* is the wire current, $\rho$ is the linear resistance of the wire (18.5 $\Omega$/m), *d* is the wire diameter (0.25mm) and *h* is the convection coefficient (75 W/(m²K)). Calculating from (2) the dissipated heat and dividing it for the volume of the wire, it is possible to estimate the power density S needed to obtain a fixed temperature increase $\Delta T$:

$$S=\frac{4\rho I^2 L}{\pi d^2 L}=\frac{4\Delta T h}{d}$$

(3)

As for example, a temperature increase of the wire of 20K needs a power density S equal to $24\cdot 10^6$ W/m³. This was the value that has been assumed to perform the initial numerical simulations.

## 3. Numerical results

A transient thermal analysis was carried out applying the power density S previously calculated for a time of 10 s. The analysis was then continued up to the stationary condition to evaluate the cooling phase. The thermal map on the model surface at the end of the heating and the spatial distribution of the temperature along the axis orthogonal to the wire is reported in Fig. 3. The same result for the frontal section of the model is reported in Fig. 4.
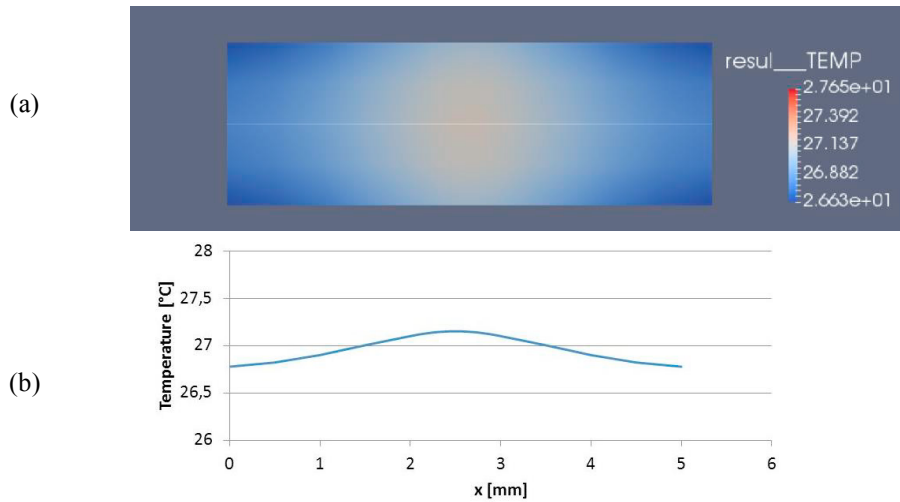


Fig. 3. Temperature map (a) and temperature distribution (b) on the top surface at the end of heating.
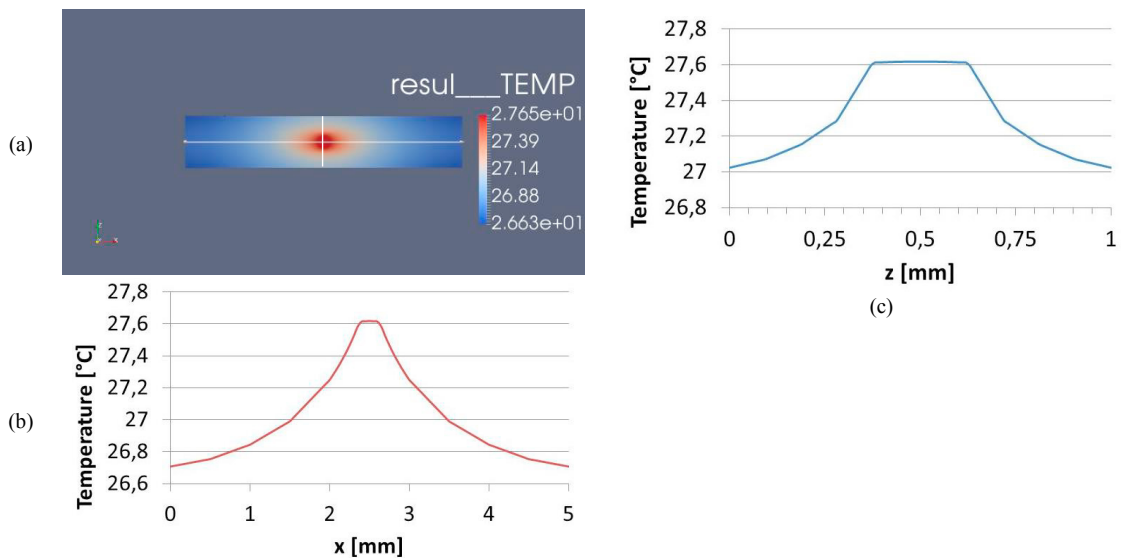


Fig. 4. Temperature map (a) and temperature distribution (b), (c) on the front surface at the end of heating.

As evident, the temperature variation induced by the applied thermal source is of about 7-8 K, which is coherent with the expected values for the damage detection application. Therefore, in order to verify the temperature variation versus the heat input, several heat power density values were applied to the SMA. In particular, five different values were considered: $12 \cdot 10^6$ W/m$^3$, $24 \cdot 10^6$ W/m$^3$, $36 \cdot 10^6$ W/m$^3$, $48 \cdot 10^6$ W/m$^3$ and $60 \times 10^6$ W/m$^3$. As expected, the

temperature increase is proportional to the power source used and can be evaluated following the evolution against time of the central point of the model. The cooling curves obtained for the five values of power density are reported in Fig. 5. The highest value of the power density produce a maximum temperature of about 39 °C, which has to be considered the maximum value applicable in order to avoid the phase transformation of the SMA wires, since the martensite transformation of Flexinol SMA wires happens at a temperature of 40°C. In order to analyse the influence of fibers orientation, several laminate models having different orientation of plies were implemented. In particular, angles of 30°, 45° and 90° were considered. As shown in Fig. 6 for the highest heat input, the fibers orientation is a significant factor on the heat transfer phenomenon causing not only different superficial temperatures in the laminate but also a different spatial distribution of the maximum temperature, which is strongly influenced by fiber orientation rather than SMA wire localization.
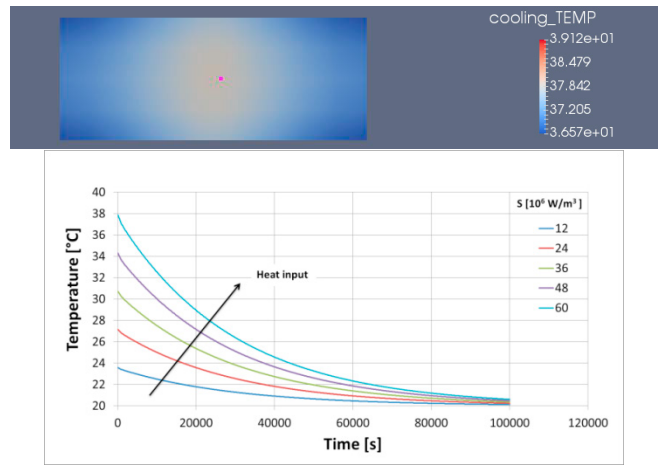


Fig. 5. Top view of the model for the power source $S = 60 \times 10^6$ W/m$^3$ and the cooling curves for all the heat input values.
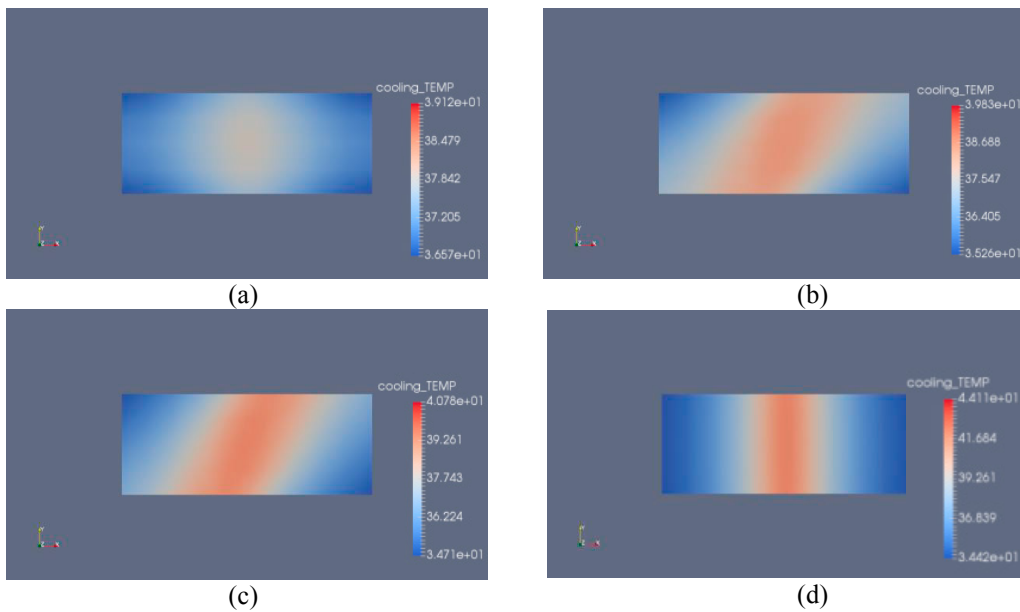


(a)

(b)

(c)

(d)

Fig. 6. Top view of the model for the power source $S = 60 \times 10^6$ W/m$^3$ and different fibers orientation: (a) 0°, (b) 30°, (c) 45°, (d) 90°.

Since the reliability of the first numerical model has been verified, a larger model was implemented consisting of a 0° laminate having 45x18x8 mm dimensions and three embedded SMA wires. This model was obtained as repetition of a scaled unit cell along the x and y directions. The definition of the material thermal properties was the same for the unite cell except for the heat convection transfer coefficient h that resulted in this case equal to 5.10 W/(m²K) according to the formula (1) and considering a more realistic $\Delta T = 10$ K. Also in the case of the composite model with three SMA wires, arising heat power density values were applied: $24 \times 10^6$, $35 \times 10^6$, $45 \times 10^6$, $55 \times 10^6$ W/m³. Fig. 7 reports the top view of the model for these values of heat input at the end of heating step (t=10s). Moreover, the influence of the heating time was analyzed increasing the heating time up to 40s. The heating curves calculated on the central point of the top surface are reported in Fig. 8 for all the values of power density S.
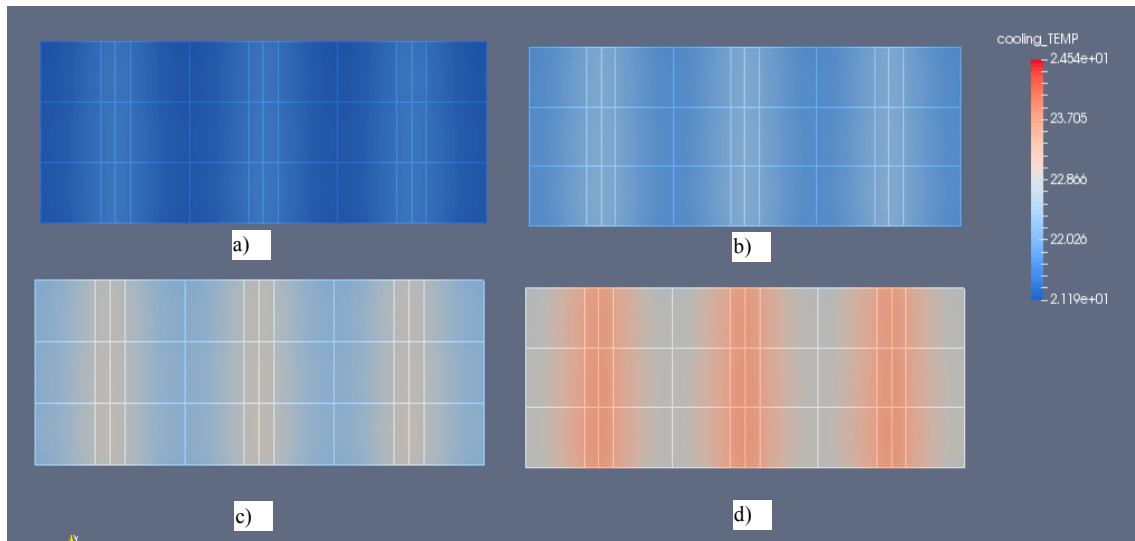


Fig. 7. Top view of the model with 3 embedded SMAs at time t=10s for power densities S=$24 \cdot 10^6$ a), $35 \cdot 10^6$ b), $45 \cdot 10^6$ c), $55 \cdot 10^6$ W/m³ d).
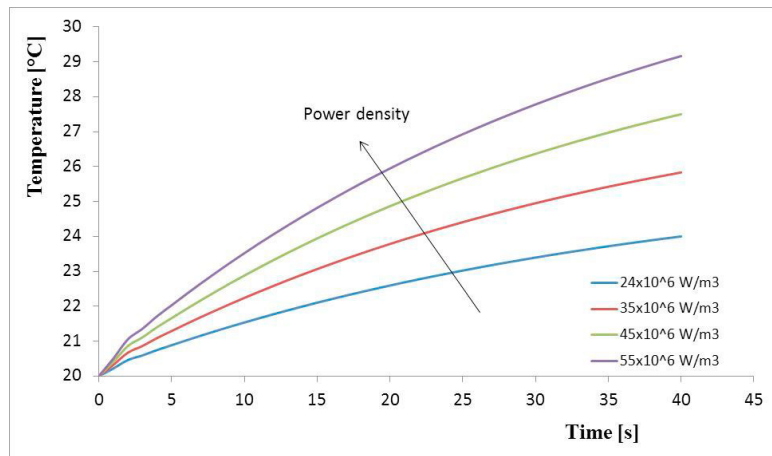


Fig. 8. Heating curves for all the heat input values on the central point of the top surface.

## 4. Experimental validation

The reliability of the presented model was verified measuring the thermal response of a GFRP panel embedded with two grids of SMA wires. In detail the panel has dimension of 210 x 300 mm and an overall thickness of about 8 mm. The panel is constituted by 8 plies having a common orientation of 0°, which corresponds to the vertical

direction of the drawing reported in Fig. 9. The representative panel contains two orthogonal grids of SMA wires having a step of 15 mm: the vertical one is positioned in correspondence of the half middle of the panel thickness, while the horizontal one is positioned between the second and third ply of the panel.

Using a stabilized electrical power source, an electrical tension of 16.5 V was applied to the vertical grid, which determines a current of 314 mA. The corresponding power source is equal to $7x10^6$ W/m$^3$. In order to produce an acceptable heating, this current was applied for a time of 120 s. The thermal map caused by the Joule effect was monitored using the infrared thermocamera FLIR 7550 and is represented in Fig. 10 at the end of the heating phase (t=120s). It is possible to observe that the Joule effect produced a $\Delta T$ equal to about 1.5 K with respect to the environmental temperature (T = 26.2°C). However, the resulting thermal map in the cooling phase is highly uniform, as showed by the aspect of the thermal map and the spatial temperature trend after 30s, 60s and 100 s (Fig. 11). This circumstance is expected to enhance the possibility to detect more easily and a with a better accuracy internal defects of the laminate.



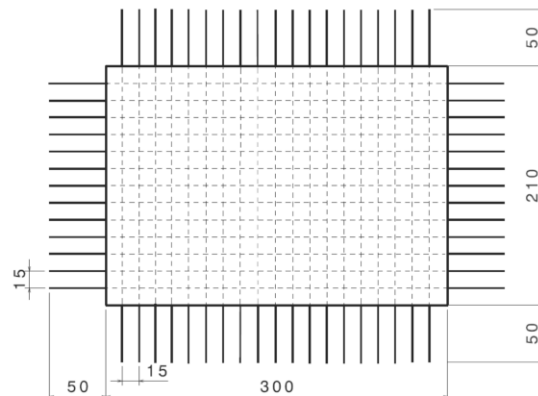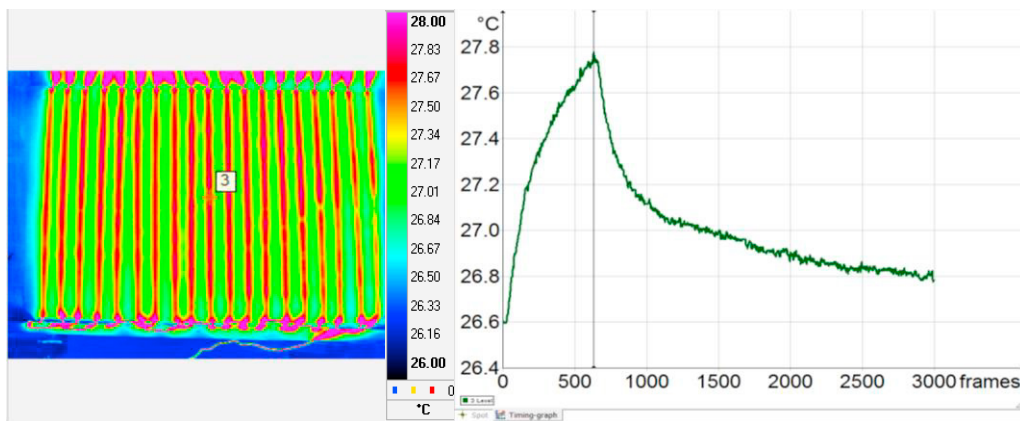Fig. 9. Geometry of the panel with indication of the SMA wire grids



(a)                                                                                              (b)

Fig.10.  GFRP real panel a), thermograms at the end of heating b), temperature vs time during heating and cooling phase of point 2

Finally, the heat input of the numerical model was settled coherently with the data of the experimental test. In particular the power source S = $7x10^6$ W/m$^3$ was applied for a time of 120 s. The map and the temperature distribution along a line on top surface are shown in Fig. 12 at t=120s. In the same Figure, the temperature evolution on the marked point in the heating and cooling phases is reported. In this case the maximum temperature increase on the surface at the end of heating phase is equal to 1.75 K, which is in good agreement with the experimental data.
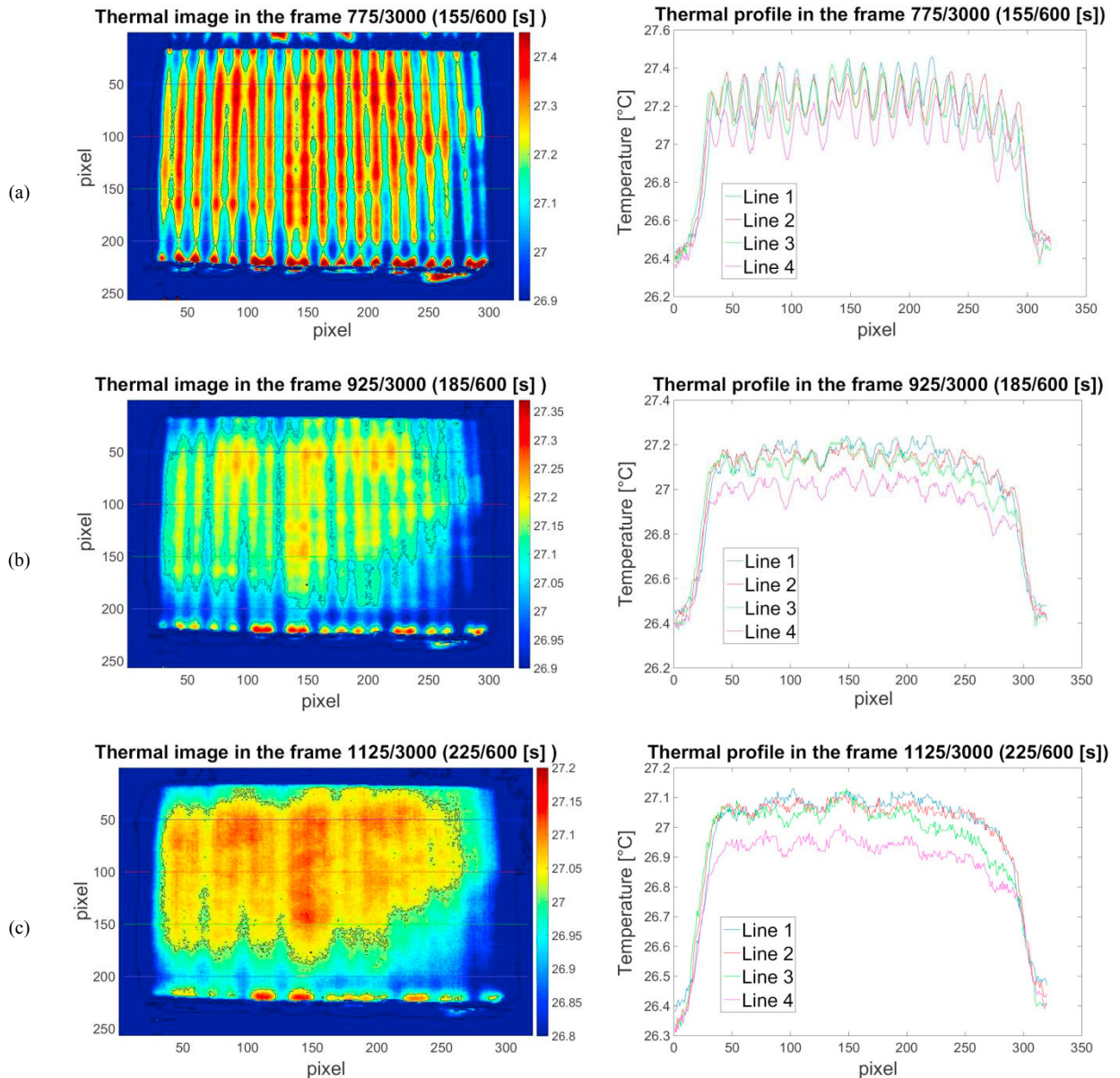
Fig.11. Experimental thermal map and temperature profile during cooling phase after: a) 30 s, b) 60s, c) 100 s

## 5. Conclusion

The technical possibility to use SMA wires as internal heat sources to detect defects in real structures made of GFRP has been verified both from a numerical and experimental point of view. Numerical simulation has been used to establish the values of power sources to be used for a correct analysis and to establish the effect of various parameters on the thermal map during heating and cooling phase. The numerical predictions have been successfully verified using a simple thermal setup. The thermal map results to be highly regular without particular care of the experimental set-up.
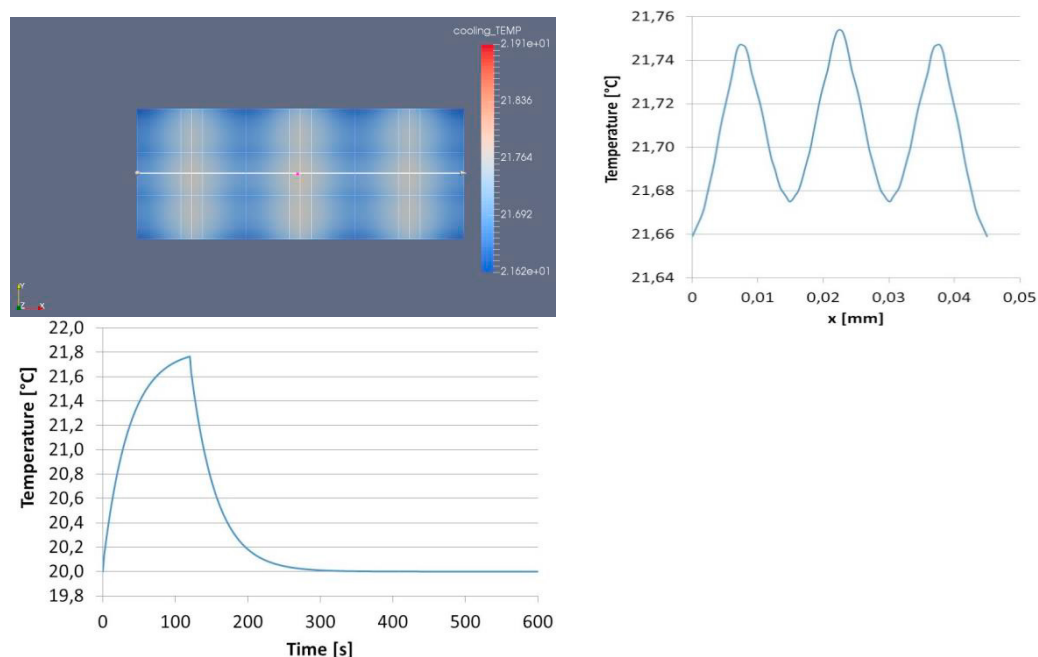
Fig.12. Temperature distribution on top surface for heat input equal $7 \cdot 10^6$ W/m$^3$ and a heating time of 120s.

## Acknowledgements

## References

Angioni, S.L., Ciampa, F., Pinto, F., Scarselli, G., Almond, D.P., Meo, M., 2016. An Analytical Model for Defect Depth Estimation Using Pulsed Thermography, Experimental Mechanics, 56, 6, 1111–1122.

Angioni, S.L, Meo, M., Foreman, A, 2011. Impact damage resistance and damage suppression properties of shape memory alloys in hybrid composites—a review, Smart Materials and Structures 20.

Bai, Y., Vallée, T., Keller, T., 2008. Modeling of thermal responses for FRP composites under elevated and high temperatures, Composites Science and Technology, 68, 1, 47-56

Cui, D., Song, G., Li, H., 2010. Modeling of the electrical resistance of shape memory alloy wires, Smart Materials and Structures;19(5).

Carslaw, H.S, Jaeger, J.C, 1959. Conduction of heat in solids, ClarendonPress.

Dattoma, V., Palano, F., Panella, F.W., 2013. Confronto numerico-sperimentale per il controllo termografico di laminati GFRP, 42° Convegno Nazionale AIAS, 11-14 Settembre 2013, Salerno, Italy.

Flexinol ® Technical and Design Data, 2018, available on-line at www.dynalloy.com

Gorbet, R.B., Wang, D.W.L, Morris, K.A., 1998. Preisach Model Identification of a 2-Wire SMA Actuator, Proceedings of the 1998 ICRA, pp. 2161-2167.

Krasnoshchekov, E., Sukomel, A., 1978. Problems in Heat Transfer, Mir Publishers, Moscow.

Ma, H.L., Gao, X., Culham, R., Gorbet, R., 2009. Temperature Measurement of shape memory alloy wires with spot welded thermocouples, Cansmart 2009, International Workshop Smart Materials and Structures, Montreal, Canada.

Maldague, X.P., 2002. Introduction to NDT by active infrared thermography, Mater Eval; 60(9):1060–73.

McLaughlin, P, McAssey, E, Deitrich, R, 1980. Non-destructive examination of fibre composite structures by thermal field techniques, NDTInt;13(2):56–62.

Mallick, P.K., 2007. Fiber-Reinforced Composites Materials, Manufacturing, and Design, Third Edition, CRC Press, Taylor & Francis Group.

Nagai, H., Oishi, R., 2006. Shape memory alloys as strain sensors in composites, Smart Materials and Structures;15(2):493.

Oishi, R., Nagai, H., 2005. Strain sensors of shape memory alloys using acoustic emissions, Sensors Actuators A: Phys;122(1):39–44.

Pickering, S., Almond, D., 2008. Matched excitation energy comparison of the pulse and lock-in thermography NDE techniques, NDT&EInt; 41(7):501–9.

Pinto, F., Maroun, F.Y., Meo, M., 2014. Material enabled thermography, NDT&E International 67, 1–9.